Journal of Power Sources 195 (2010) 1543–1550

Contents lists available at ScienceDirect

Journal of Power Sources

journal homepage: www.elsevier.com/locate/jpowsour

Self-rising synthesis of Ni–SDC cermets as anodes for solid oxide fuel cells

Qiang Liu [a], Xihui Dong [a], Chenghao Yang [a], Shuguo Ma [b], Fanglin Chen [a,*]

[a] Department of Mechanical Engineering, University of South Carolina, 300 Main Street, Columbia, SC 29208, United States
[b] College of Engineering and Computing, University of South Carolina, Columbia, SC 29208, United States

ARTICLE INFO

Article history:
Received 19 August 2009
Received in revised form
28 September 2009
Accepted 30 September 2009
Available online 20 October 2009

Keywords:
Solid oxide fuel cells (SOFCs)
Anode material
Ni–SDC cermets
Self-rising synthesis
Porous
Nanocrystals

ABSTRACT

Ni–SDC cermets have been obtained using a self-rising approach by two different ways, one-step direct synthesis (OS) and ball milling the separately prepared NiO and SDC powders (BM). The results showed that self-rising approach was an efficient way for the synthesis of porous materials composed of evenly distributed uniform size nanocrystals. The as-synthesized powders have been applied as anodes for solid oxide fuel cells, whose electrochemical properties have been systematically studied. Cells with anodes from the BM method showed better performance compared with those of the OS method, achieving a maximum power density of 400 mW cm^{-2} at 600 °C.

© 2009 Elsevier B.V. All rights reserved.

1. Introduction

Solid oxide fuel cells (SOFCs) convert chemical energy from the fuel directly to electricity, offer high system efficiency and are environmentally benign [1]. While the existing SOFC technology has demonstrated much higher chemical to electrical energy conversion efficiency (50%) with minimal pollutant emission over conventional energy conversion technologies (16–34%), the cost of the current SOFC system is still prohibitive for wide commercial applications. The cost of SOFC technology can be dramatically reduced by reducing the operating temperature to 400–600 °C so that relatively inexpensive metallic components can be used as interconnect, heat exchangers, and other structural components of the SOFC system [2]. A lower operating temperature would also ensure a greater overall system stability, reliability, efficiency and a reduction in the thermal stresses in the active ceramic structures, leading to a longer expected lifetime for the system. Ceria-based solid solution, especially Sm_2O_3 doped CeO_2 ($Sm_{0.2}Ce_{0.8}O_{1.9}$, SDC) has been regarded as the most promising electrolyte for low temperature SOFCs because of its excellent oxygen ion conductivity compared to yttria stabilized zirconia (YSZ) [3]. Correspondingly, the most suitable anode for SDC electrolyte-based SOFCs would be Ni–SDC cermets [4].

The performance of an SOFC depends strongly on the anode microstructure and it is critical to consider how the anode works on a microscopic scale. The electrochemical reaction can only occur at the three-phase boundary (TPB) region [5], which is defined as the location where the electrolyte (SDC), electrocatalyst (Ni), and gas phase all come together. Therefore, how to increase the TPB length as much as possible in the limited effective anode volume would be the key point to improve the electrochemical performance at lower cell operating temperatures. For the TPB enlargement, optimization of the anode microstructure by decreasing the particle size to increase the surface area would be a feasible approach [6].

Our previous work has shown that self-rising method is an effective way to obtain porous powders composed of nanocrystal aggregates with high surface areas [7], which are considered beneficial for further enlargement of the TPBs of the Ni–SDC cermet anode, thus improving the anodic performance. Given the above considerations, in this report, Ni–SDC anode powders have been obtained by a self-rising technique using two different ways: the first strategy is the in situ one-step synthesis (noted as OS); another pathway is mixing the separately prepared NiO and SDC powders together by ball milling (noted as BM). Anode-supported cells are pressed using these two different types of powders and their electrochemical properties have been systematically studied.

2. Experimental

2.1. Synthesis of powder

The NiO–SDC composites (50 mol% NiO) were synthesized by self-rising approach [8]. $Sm(NO_3)_3{\cdot}6H_2O$, $Ce(NO_3)_3{\cdot}6H_2O$ and $Ni(NO_3)_2{\cdot}6H_2O$ were used as metal precursors. Polyvinyl alcohol

* Corresponding author. Tel.: +1 803 777 4875; fax: +1 803 777 0106.
E-mail address: chenfa@cec.sc.edu (F. Chen).

0378-7753/$ – see front matter © 2009 Elsevier B.V. All rights reserved.
doi:10.1016/j.jpowsour.2009.09.071

(PVA) was used as fuel and binder and urea was chosen as the leavening agent. For one-step synthesis, three metal precursors were dissolved in hot water together with PVA and urea at the same time, and then the solution was dried in an oven at 50 °C. The dried precursor was then taken into a furnace for calcination. The heating rate was 1 °C min^{-1} to 160 °C. After dwelling at 160 °C for 3 h, it was heated to 500 °C and held for another 5 h, resulting in NiO–SDC composite powders by one-step synthesis (OS). For comparison, SDC and NiO powders were also prepared by self-rising approach separately. They were then mixed together by ball milling for 5 h (BM). The electrolyte SDC and cathode $La_{0.6}Sr_{0.4}Co_{0.2}Fe_{0.8}O_3$ (LSCF) powders were synthesized through the glycine-nitrate-process (GNP) [9].

2.2. Cell fabrication

Anode-supported single cells were fabricated by one-step dry-pressing method. Green bodies consisting of NiO–SDC substrates and SDC electrolytes were formed by co-pressing the anode powder and SDC powder uniaxially under 200 MPa. The anode and electrolyte bilayer (13 mm in diameter) were then co-fired at 1350 °C in air for 5 h at a ramping rate of 2 °C min^{-1} to densify the SDC film. A slurry consisting of LSCF and a Heraeus binder V006 (weight ratio of 1:1) was then applied to the electrolyte by screen-printing, and then fired at 1000 °C in air for 3 h to form a porous cathode. The resulting coin shaped cathode had a thickness of 20 μm and an effective area of 0.33 cm^2. Platinum slurries (Haraeus C8829) were brushed on the cathode side as current collector. The fabrication of cathodes for all cells tested in this study was kept as consistent as possible so that the cathodic polarization resistances of all cells were relatively consistent.

The single cell was sealed on an alumina tube with silver paste (DAD-87, Shanghai Research Institute of Synthetic Resins) [9]. The cathode side was open to air, and the anode side was exposed to H_2 at a flow rate of 40 mL min^{-1}, detailed cell test structure can be found in previous report [9]. The cell was heated to 600 °C and NiO was reduced to Ni in situ. The cell was stabilized at 600 °C for 2 h before the electrochemical test was performed. Electrochemical characterizations were performed at temperatures from 450 to 600 °C under ambient pressure. Three tests were recorded at each temperature to get an average value. Fuel cell performance was measured with a Versa STAT 3-400 test system (Princeton Applied Research). Hydrogen (3% H_2O) was used as fuel and stationary air as oxidant. AC impedance was measured at open cell circuit in the frequency range from 0.05 Hz to 100 kHz on a potentiostat/galvanostat with built-in impedance analyzer.

2.3. Characterization

The powder X-ray diffraction (XRD) pattern was recorded on a D/MAX-3C X-ray diffractometer with graphite-monochromatized CuKα radiation (λ = 1.5418 Å), employing a scan rate of 5° min^{-1} in the 2θ range of 10–80°. The microstructure and morphology of the synthesized product were characterized by scanning electron microscopy (SEM, FEI Quanta 200) equipped with an energy dispersive X-ray (EDX) analyzer and transmission electron microscopy (TEM, Hitachi H-800, 200 kV). High resolution TEM (HRTEM), selected area electron diffraction (SAED) and EDX line scan were conducted using a JEOL 2011. X-ray photoelectron spectroscopy (XPS) was conducted on a Kratos Axis Ultra DLD instrument. The samples were also characterized by nitrogen adsorption/desorption at −196 °C by using a NOVA 2000 series volumetric adsorption system. Simultaneous thermal analysis (thermogravimetry–differential scanning calorimetry, TG–DSC) was performed on a NETZSCH STA 409. Data were collected between room temperature and 500 °C at a heating rate of 2.5 °C min^{-1} under air atmosphere.

3. Results and discussions

3.1. Synthesis of cermets powders by self-rising approach

Self-rising, particularly referring to self-rising flour, was firstly invented in food industry [10]. Due to the preloaded leavening agent inside the flour, a nice lift can be achieved in the baked products. Inspired by this strategy that can easily introduce pores into the bulk materials, we developed the novel self-rising approach, which has been described in our previous report in detail [8]. Briefly speaking, PVA as a binder with metal precursor can be regarded as the dough, and urea is chosen as the leavening agent. During the heating process urea will decompose, releasing gases to make the elastic PVA binder sharply expand. Upon even higher temperature calcination, PVA frames will be burnt off, resulting in loose packed porous metal oxide powders with extremely low filled density. Using this method, we have successfully obtained porous pure phase metal oxides such as SDC and Fe_2O_3 [8]. To illustrate the

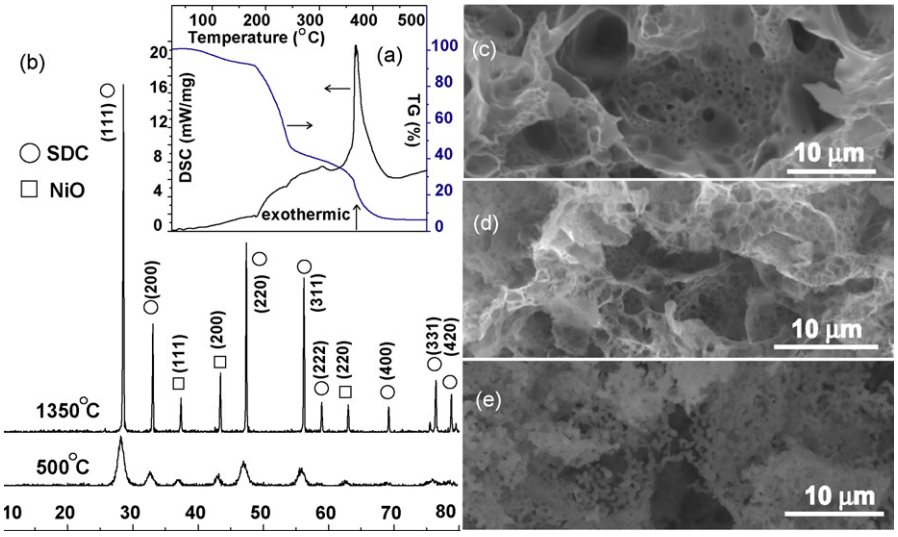

Fig. 1. (a) TG–DSC and (b) XRD of sample OS; SEM of sample OS after different temperature calcinations (c) 500 °C, (d) 750 °C and (e) 1350 °C.

wide applicability of the self-rising approach, we will describe the synthesis and characterization of mixed NiO–SDC composites by one-step synthesis.

The simultaneous TG–DTA curves of the gel precursor of sample OS in flowing air are shown in Fig. 1a. The TG curve displays two drastic weight losses, one is around 160 °C and another is at 360 °C. The first weight loss can be attributed to the urea decomposition. Therefore, this temperature was chosen as a dwelling temperature during the heat-treatment step to ensure that the self-rising process is slow and complete. The latter one is related to the combustion of PVA binder, accompanied by a strong exothermic peak at the same temperature in the DSC curve. No further weight loss could be observed after 450 °C, suggesting formation of crystalline NiO and SDC, which is consistent with the subsequent XRD analysis. Shown in Fig. 1b is the XRD analysis graph. Upon 500 °C calcination for 5 h, all the diffraction peaks can be perfectly indexed as NiO and SDC respectively. Fine grain size of the SDC powder can be expected from the very wide diffraction peaks in the XRD pattern of the 500 °C calcined sample. The strong and sharp diffraction peaks for the sample upon firing at 1350 °C indicate that the obtained product is highly crystallized and sintered large particles have formed. No other phases can be detected upon the high temperature firing except NiO and SDC phases.

The SEM graph of the sample OS after 500 °C calcinations (Fig. 1c) displays foam-like structure with randomly distributed macropores in diameter around several microns. The as-synthesized products exhibit extremely low filled density due to the large amount of voids inside, which would be beneficial for mass transport. On the other hand, nitrogen adsorption and desorption isotherm displays a type IV isotherm with H1-shaped hysteresis loop (Fig. 2), indicating that the final materials belong to a mesoporous family, with pore size close to 4.0 nm. The Brunauer–Emmett–Teller (BET) surface area and pore volume of sample OS after 500 °C calcinations are 38 $m^2 g^{-1}$ and 0.054 $cm^3 g^{-1}$, respectively. Large surface area is expected to improve gas diffusion and enlarge the TPB region. Similar porous structure can be retained even after 750 °C calcinations (Fig. 1d). Upon 1350 °C heating treatment, due to the dramatic grain growth, volume shrinkage of the powders is apparent and the original macropores disappear, resulting in large particles with network-like morphology (Fig. 1e). However, the foam-like structure has not collapsed, and the retained low filled density will significantly increase the active sites for the electrode reactions, thus improving the electrochemical performance of the cell.

The single SDC powders obtained by self-rising approach also displays the similar trend in morphology evolution as a function of the firing temperatures, which has been reported by us previously [7]. The separately prepared SDC and NiO powders using the self-rising approach are mixed together by ball milling, and were then applied as anode materials for SOFCs (cell BM) and their electrical performance has been compared with that of the one-step synthesized powders (cell OS).

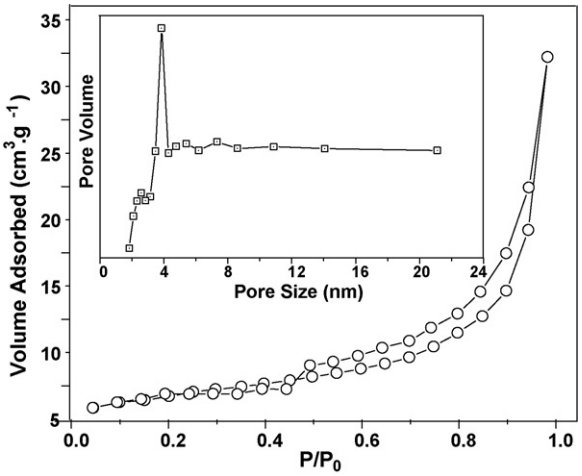

Fig. 2. BET and pores size distribution of sample OS after 500 °C calcinations.

3.2. Comparison of single cell performance

The cost-effective dry-pressing method has been adopted to fabricate anode-supported single cells. Shown in Fig. 3a and b are their cross-sectional SEM micrographs, which consist of porous Ni–SDC anode support (bottom, ~350 μm), a dense SDC electrolyte (middle, ~20 μm) and a porous LSCF cathode (top, ~20 μm). The electrolyte membranes of both samples are dense with no observable cross-layer pinholes or cracks and are well adhered to the porous Ni–SDC anode support. In contrast to the dense SDC electrolyte layer, the anode is highly porous (Fig. 3c and d) even after such high temperature firing (1350 °C), indicating that the self-rising is a promising approach for synthesis of porous electrode materials.

The voltages and power densities of the single cells as a function of current density at different operating temperatures are shown in Fig. 4. For both samples the cell voltages decrease almost linearly with increasing current density, indicating that the IR losses resulted from the ohmic resistance associated with the cell are dominating in the cell performance. The open-circuit voltage (OCV) is lower than 1.0 V, and decreases with the increase in operating temperatures since SDC becomes a mixed oxygen ionic and

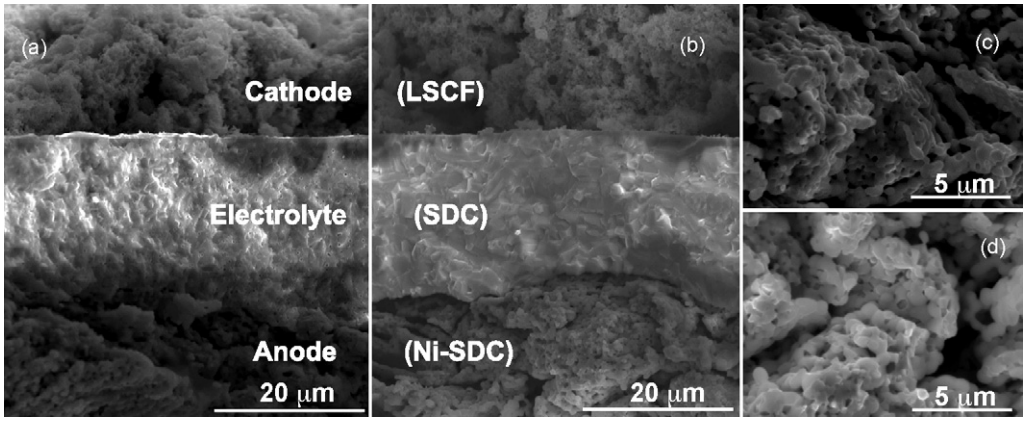

Fig. 3. Cross-sectional SEM graphs of anode-supported single cells: (a) OS, (b) BM and high magnification SEM of anode, (c) OS and (d) BM.

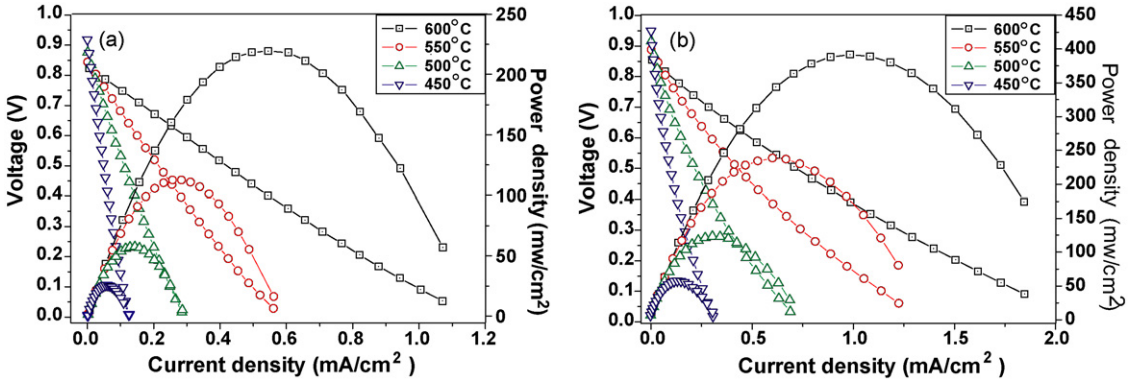

Fig. 4. I/V and I/P curves of single cells with different anode supports: (a) OS and (b) BM.

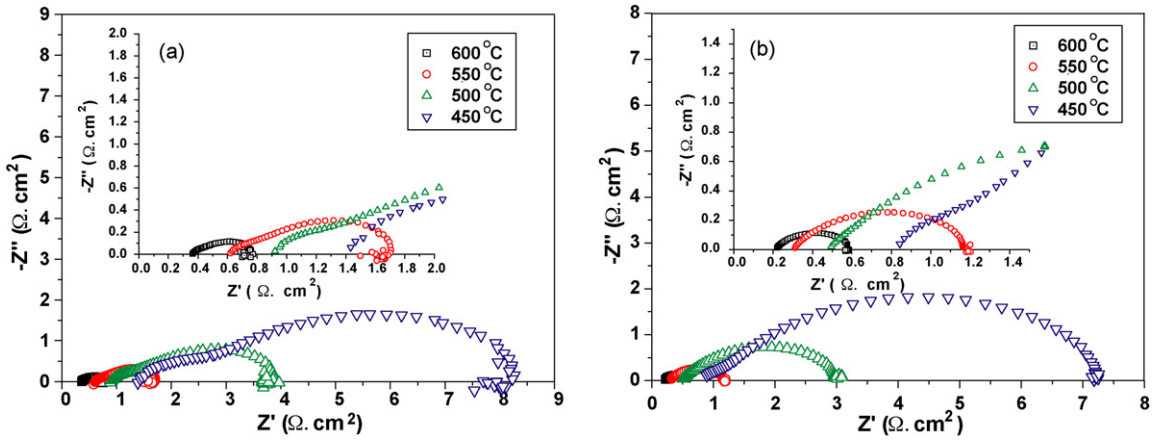

Fig. 5. Impedance spectra of single cells with different anode supports: (a) OS and (b) BM.

electronic conductor at elevated temperatures [11]. The Nernst potential predicted under the H_2 with 3% H_2O as the fuel and air as the oxidant at these temperatures exceeds 1.10 V; obviously the obtained OCVs in this work are lower than the theoretical value, but they are consistent with the reported values due to the reduction of ceria from Ce^{4+} to Ce^{3+} leading to current leakage with an n-type electronic conduction, resulting in drop in OCVs [12]. Based on previous report [13], a thinner electrolyte film would reduce the ohmic resistance, but enhance the possibility of defects in the electrolyte such as micro-cracks spanning the entire electrolyte thickness, leading to a lower OCV because of gas leakage. Although there is an average of 25 mV higher OCV for cell BM than OS, overall the OCV are almost equal and comparable to those reported in the literature for SDC-based cells operated at the same temperatures. For instance, at 600 °C, the OCV for sample BM and OS are 0.86 and 0.83 V, respectively, which are close to or even higher than the reported values (0.86 V [13], 0.87 V [14], 0.83 V [15,16] and 0.69 V [17]). The closeness in OCVs implies that dense electrolyte film has been obtained for both samples and this is in agreement with the SEM observation (Fig. 3).

It can be clearly seen that the cell BM has much better performance than cell OS at the same temperature. The maximum power density reached ~400 mW cm^{-2} for cell BM at 600 °C, which is almost twice as much as that of cell OS (~225 mW cm^{-2}), indicating the influence of different anode structure on cell performance since the electrolytes and cathodes were fabricated using the same procedures. For sample BM, the maximum power density of the cell is about 55, 125, 245 and 400 mW cm^{-2} at 450, 500, 550 and 600 °C, respectively. These results are comparable to those reported for H_2/air fuel cells with SDC electrolytes and Ni–SDC anodes [17,18].

AC impedance spectra of the cells under open-circuit conditions are plotted in Fig. 5. The ac impedance is made up of both ohmic and electrode polarization resistances. The intercept with the real axis at high frequencies is the series ohmic resistance (R_s). The arc observed between the high frequency and the low frequency can be associated with the interfacial impedance between the electrode and the SDC electrolyte (R_p) [19]. It has been reported that R_s is not only mainly attributed to the resistive contribution of the electrolyte but also strongly influenced by the arrangement of electrodes [20]. The ionic conductivity of SDC was estimated to be

Table 1
Results of single cell OS and BM operating at 450 and 600 °C.

Sample	Temperature (°C)	OCV (V)	MPD (mW cm^{-2})	R_s (Ω cm^2)	R_p (Ω cm^2)
OS	600	0.83	225	0.362	0.399
	450	0.94	25	1.424	6.829
BM	600	0.86	400	0.211	0.365
	450	0.96	55	0.813	6.422

MPD: maximum power density; R_s: Ohmic loss; R_p: electrode polarization resistance.

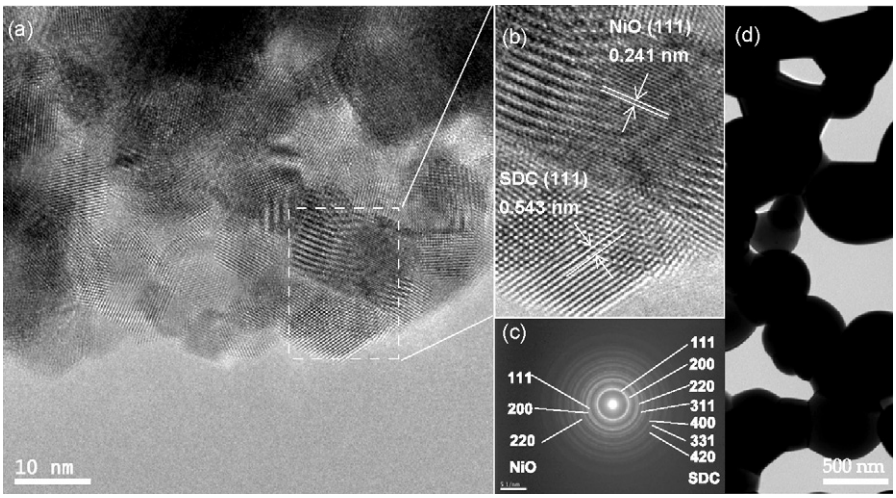

Fig. 6. (a and b) HRTEM and (c) SAED of sample OS obtained after 500 °C calcinations and (d) TEM of sample OS obtained after 1350 °C calcinations.

2.5×10^{-2} S cm^{-1} at 600 °C and 5×10^{-3} S cm^{-1} at 450 °C, respectively [21]. Consequently, the ohmic resistances should be 0.24 Ω at 600 °C and 1.2 Ω at 450 °C, based on an SDC layer thickness of 20 μm, an electrode area of 0.33 cm^2 and negligible ohmic resistance from the electrodes. As shown in Table 1, the experimental results of R_s in this work are from 0.2 to 0.4 at 600 °C and 0.8 to 1.5 at 450 °C, which are consistent to the reported values, implying that our processing method and materials have been adequately optimized [22].

The enhanced performance of sample BM supported cells than OS can also be confirmed by R_p, the cell polarization resistance from both anode and cathode are shown in Table 1. R_p increases from 0.365 for BM to 0.399 Ω cm^2 for OS at 600 °C, and from 6.422 for BM to 6.829 Ω cm^2 for OS at 450 °C. Considering the identical cathode preparation used in these experiments, any changes in the total resistance among the cells are very likely due to the differences in the anodes.

3.3. Discussions

Using the one-step co-precipitation method, Ding et al. [6] and Xia et al. [18] also successfully synthesized mixed Ni–SDC or Ni–GDC ($Gd_{0.1}Ce_{0.9}O_{1.95}$) cermets, which have been applied as anodes for IT-SOFCs. Both of them found that the one-step approach was superior to the traditional mechanical mixing method and attributed the improved performance to the homogenous anode structure which can effectively enlarge the TPB area [6]. However, our present results indicate that the cell performance of cell OS obtained by one-step self-rising combustion strategy is not as good as that of cell BM, which seems contradictory to the previous findings.

To find out the reasons for this discrepancy, HRTEM analysis on the detailed structure of sample OS is conducted. As shown in Fig. 6a and b, it can be clearly seen from the bright field images that sample OS contains aggregated nanocrystals of 5–10 nm in size. The observed lattice space, 0.241 and 0.543 nm, are corresponding to the respective NiO (1 1 1) and SDC (1 1 1) surfaces, which can be further confirmed by the selected area electron diffraction (SAED) analysis (Fig. 6c). The well crystallized nanoparticles are randomly and uniformly distributed, resulting in a relatively high BET surface area (38 m^2 g^{-1}) as mentioned previously (Fig. 2). Consequently, it would have large TPB length which would be beneficial to cell performance. However, the double layer (electrolyte and anode support) must be sintered at high temperature (1350 °C) to make a dense electrolyte film. Due to the high surface energy of the nanocrystals, it would be difficult to retain the original porous structure and a dramatic grain growth is unavoidable during the sintering process (Figs. 6d and 1e). Therefore, the uniformly distributed NiO and SDC nanoparticles would have disadvantage compared to large particles in the sintering process instead, since they tend to aggregate and sinter together to evenly distributed Ni–SDC solid solution, resulting in the formation of core-shell like structure after hydrogen treatment, which has been further confirmed by the following EDX line scan experiments.

It has been widely accepted that for Ni–SDC anodes, Ni particles would not only catalyze breaking of the H_2 bond but also provide electronic conduction from the reaction site to the current collector. SDC would function as the ion (O^{2-}) transport path from the electrolyte, and the electrochemical reaction can only occur at the Ni–SDC-gas TPB site (Scheme 1) [23]. However, the core–shell structure would dramatically decrease the TPB area in the electrode. Either encapsulation of SDC or Ni particles will dramatically deactivate the anode catalysts; in the former case,

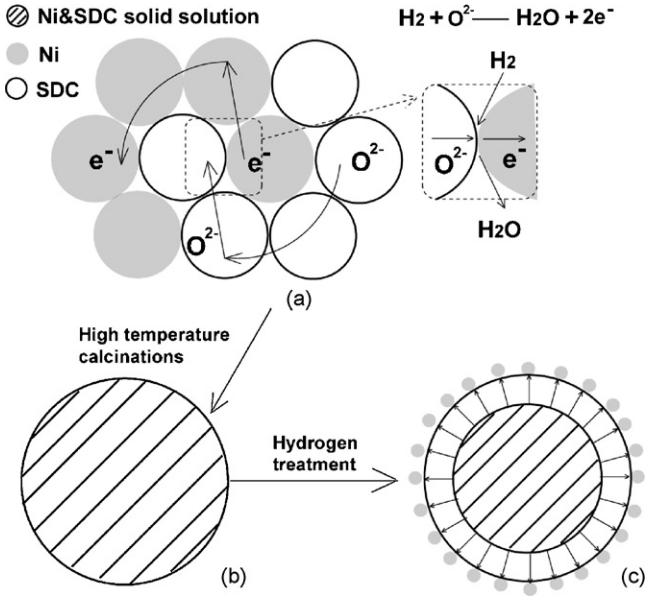

Scheme 1. (a) Schematic of the Ni/SDC anode TPB; (b) even-distributed solid solution obtained after high temperature calcinations of aggregated Ni and SDC nanocrystals; (c) small nickel particles begin to separate out during the hydrogen pretreatment.

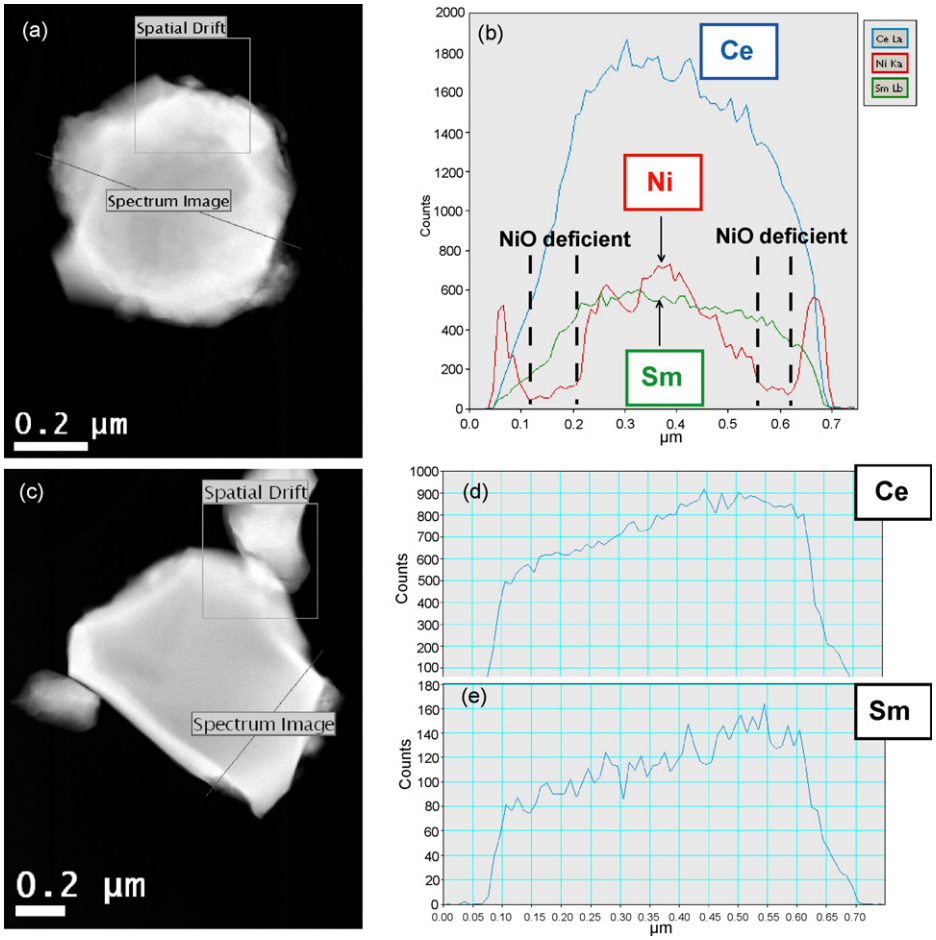

Fig. 7. (a) TEM and (b) EDX line scan of particle OS; (c) TEM and (d and e) EDX line scan of particle BM from tested cells.

ionic conduction will disappear, while in the latter case, electronic conductivity and the ability of catalytic H_2 decomposition will be greatly reduced. The EDX line scan test can help determine which type of encapsulation has been formed during the sintering process. As shown in Fig. 7, after 1350 °C calcinations, dramatic growth has been detected for both samples: the average particles size are much bigger, around 0.7–1 μm (Fig. 7a and c). For sample OS, the EDX line scan result (Fig. 7b) indicates that the exterior surface of the particles is covered by a thin layer (about 20 nm) of Ni, followed by a thicker SDC shell (~100 nm), while the inside core is a mixture of SDC and Ni. King et al. [24] have reported that NiO would be dissolved into the YSZ to form a solid solution during the high temperature sintering step, and then separated out to form small Ni particles under pretreatment in hydrogen. The very outside Ni layer should be formed through this way (Scheme 1). Meanwhile, large ratio of NiO particles has been encapsulated by the SDC layer, which would lose the anode catalytic activity and thus have negative influence on the cell performance.

It should be noted that the sample BM has a distinct morphology features compared to that of OS, as displayed in Fig. 7d and e, only Ce and Sm have been found and no Ni signal has been detected in the SDC particle, similarly no Ce or Sm elements has been found in the Ni particles of sample BM. Such a morphological difference in the starting particles can, in turn, influence variations in anodic performance. As shown in Fig. 5, the bulk resistance of cell OS is significantly larger than that of cell BM, and the difference is greater when the temperature is lower. Based on the similar electrolyte and cathode structure of both cells, the poor cell performance of cell OS might suggest too much SDC present in the anode due to the core–shell anode structure.

This kind of deactivation mechanism has also been observed in other catalyst system such as nano-dimensional gold particles deposited on ceria (Au/CeO_2) for low temperature CO oxidations. Recent study indicates that co-precipitation method for catalyst preparation is significantly inferior [25,26] because large ratio of Au catalysts is encapsulated inside the CeO_2, thus substantially decreasing their catalytic activity [25].

For cell BM, it is difficult to get an evenly distributed mixture of Ni–SDC nanocrystals by ball milling. Therefore the powders after high temperature sintering cannot form large quantities of core–shell structure, as shown in Fig. 8c and d. EDX mapping (Fig. 8d) for Ni element from the BM anode pellet after sintering at 1350 °C reveals island distribution of Ni and SDC, i.e. a separation of Ni and SDC particles is observed. However, for cell OS (Fig. 8a and b), the Ni elements are evenly distributed from EDX mapping analysis (Fig. 8b), suggesting that a continuous and uniform nickel distribution in sample OS, and it is difficult to identify Ni and SDC particles, which may be caused by the severe encapsulation with each other. It seems that for one-step self-rising synthesis, the common advantage for nanocrystal catalyst does not exist. On the contrary, it has adverse effect on cell performance due to the core–shell structure by high temperature sintering. In addition, the increased number of grain boundaries in the OS sample may be influencing conductivity, particularly if the ionic conductivity is boundary diffusion limited. For Ding and Xia's co-precipitation preparation of Ni–SDC cermets, the as-synthesized particles are much larger (50–100 nm) than those in this work [6,18]. Therefore, high temperature sinter-

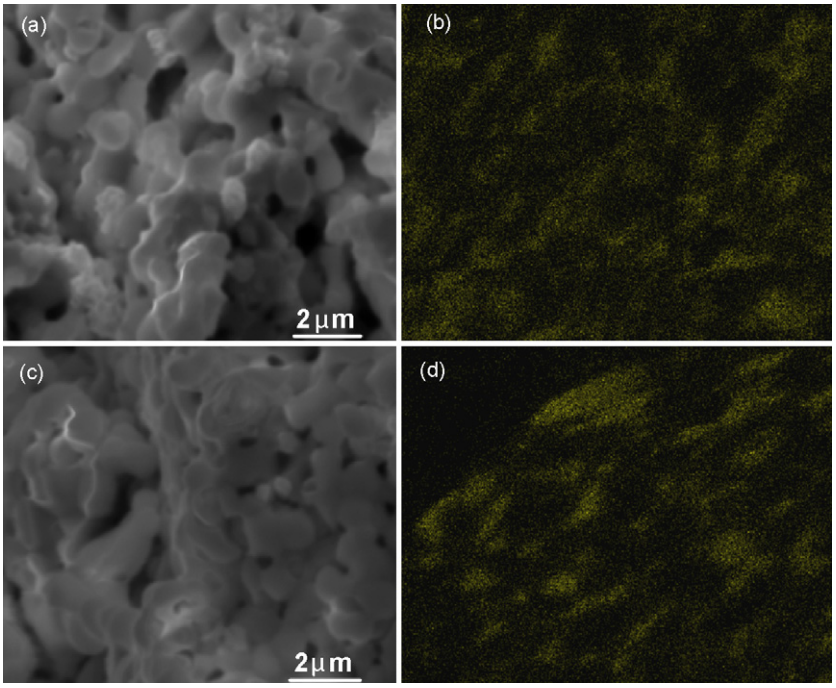

Fig. 8. SEM and EDX mapping (Ni) for tested cell OS (a and b); cell BM (c and d).

ing of the electrolyte/anode has not induced the formation of evenly distributed solid solution and the subsequent core–shell framework, and the separately well-attached Ni–SDC particles would thus increase the TPB length, resulting in enhanced cell performance compared with that of the cells prepared by the mechanical mixing method.

Another reason for the weak performance of cell OS can be attributed to the reaction between NiO and SDC through the following reaction [27]:

$$NiO \xrightarrow{CeO_2} Ni''_{Ce} + V^{\bullet\bullet}_{O} + O^{x}_{O} \quad (1)$$

XPS analysis of both samples (Fig. 9) reveal that for sample BM before and after the H_2 reduction, the binding energy of Ni^{2+} and Ni^0 is very close to the theory value, suggesting that their electronic structures are similar to that of the bulk material. However, for sample OS, the binding energy of Ni $2P_{3/2}$ has shifted to lower values compared to that of a pure phase, which may be caused by reaction between Ni and SDC during the high temperature sintering. The evenly distributed NiO and SDC nanocrystals (Fig. 6a) in sample OS significantly increase the probability of the diffusion of Ni into SDC, making their reaction much easier than that of sample BM. Mori et al. have confirmed that Ni indeed has a contribution to the concentration and ordering of oxygen vacancies (reaction (1)), which will lead to a degradation of the ionic conductivity and cell performance [27].

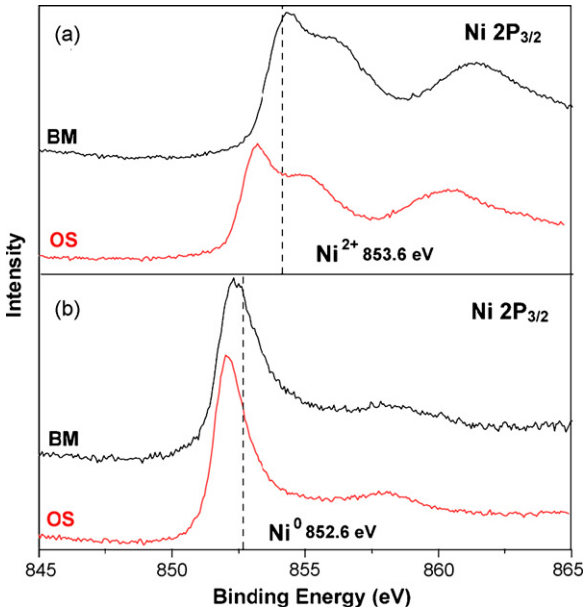

Fig. 9. Ni $2P_{3/2}$ XPS spectra of sample BM and OS before (a) and after (b) H_2 reduction. The dash lines indicate the theory peak value of Ni^{2+} and Ni^0, respectively.

4. Conclusions

Based on the above analysis, the following conclusions can be obtained:

(1) Self-rising approach is an efficient way for the synthesis of porous materials. The obtained products show high BET surface area with small and evenly distributed nanocrystals. Such porous material is suitable as catalyst which does not involve extremely high temperature processing and operating environment.
(2) Compared to cell BM, cell OS shows sluggish anode performance, which may be attributed to the core–shell structure formed during the high temperature sintering in hydrogen atmosphere that blocks the electron or oxygen ion transport. Another reason for the reduced performance of cell OS may be due to Ni diffusion to the SDC particles, leading to the degradation of the ionic conductivity.

Acknowledgments

The financial support of the Department of Energy (contract no. DE-FG36-08GO88116) and the South Carolina Space Grant Consortium is acknowledged gratefully.

References

[1] R.J. Gorte, J.M. Vohs, Curr. Opin. Colloid Interface Sci. 14 (2009) 236–244.
[2] D.J.L. Brett, A. Atkinson, N.P. Brandon, S.J. Skinner, Chem. Soc. Rev. 37 (2008) 1568–1578.
[3] M. Mogensen, N.M. Sammes, G.A. Tompsett, Solid State Ionics 129 (2000) 63–94.
[4] H. Kishimoto, K. Yamaji, T. Horita, Y.P. Xiong, M.E. Brito, M. Yoshinaga, H. Yokokawa, Electrochemistry 77 (2009) 190–194.
[5] S. McIntosh, R.J. Gorte, Chem. Rev. 104 (2004) 4845–4865.
[6] C.S. Ding, H.F. Lin, K. Sato, T. Hashida, Scripta Mater. 60 (2009) 254–256.
[7] Q. Liu, F. Zhao, X.H. Dong, C.H. Yang, F. Chen, J. Phys. Chem. C 113 (2009) 17262–17267.
[8] Q. Liu, F. Chen, Mater. Res. Bull. 44 (2009) 2056–2061.
[9] F. Zhao, Z.Y. Wang, M.F. Liu, L. Zhang, C.R. Xia, F. Chen, J. Power Sources 185 (2008) 13–18.
[10] M. McCamish, J. Chem. Educ. 64 (1987) 710–712.
[11] K. Eguchi, T. Setoguchi, T. Inoue, H. Arai, Solid State Ionics 52 (1992) 165–172.
[12] B.C.H. Steele, Solid State Ionics 129 (2000) 95–110.
[13] X.G. Zhang, M. Robertson, S. Yick, C. Deces-Petit, E. Styles, W. Qu, Y.S. Xie, R. Hui, J. Roller, O. Kesler, R. Maric, D. Ghosh, J. Power Sources 160 (2006) 1211–1216.
[14] T. Misono, K. Murata, T. Fukui, J. Chaichanawong, K. Sato, H. Abe, M. Naito, J. Power Sources 157 (2006) 754–757.
[15] D. Ding, L. Li, K. Feng, Z.B. Liu, C.R. Xia, J. Power Sources 187 (2009) 400–402.
[16] H.Z. Zhang, H.Y. Liu, Y. Cong, W.S. Yang, J. Power Sources 185 (2008) 129–135.
[17] C.J. Zhu, X.M. Liu, D. Xu, D.J. Wang, D. Yan, L. Pei, T.Q. Lu, W.H. Su, J. Power Sources 185 (2008) 212–216.
[18] X.H. Fang, G.Y. Zhu, C.R. Xia, X.Q. Liu, G.Y. Meng, Solid State Ionics 168 (2004) 31–36.
[19] W. Zhou, Z.P. Shao, R. Ran, P.Y. Zeng, H.X. Gu, W.Q. Jin, N.P. Xu, J. Power Sources 168 (2007) 330–337.
[20] W.X. Zhu, Z. Lu, S.Y. Li, B. Wei, J.P. Miao, X.Q. Huang, K.F. Chen, N. Ai, W.H. Su, J. Alloys Compd. 465 (2008) 274–279.
[21] M. Chen, B.H. Kim, Q. Xu, B.K. Ahn, W.J. Kang, D.P. Huang, Ceram. Int. 35 (2009) 1335–1343.
[22] S. Lee, Y. Lim, E.A. Lee, H.J. Hwang, J.W. Moon, J. Power Sources 157 (2006) 848–854.
[23] S.W. Tao, J.T.S. Irvine, Nat. Mater. 2 (2003) 320–323.
[24] D.L. King, J.J. Strohm, X.Q. Wang, H.S. Roh, C.M. Wang, Y.H. Chin, Y. Wang, Y.B. Lin, R. Rozmiarek, P. Singh, J. Catal. 258 (2008) 356–365.
[25] M.A. Centeno, M. Paulis, M. Montes, J.A. Odriozola, Appl. Catal. B 61 (2005) 177–183.
[26] A.M. Venezia, G. Pantaleo, A. Longo, G. Di Carlo, M.P. Casaletto, F.L. Liotta, G. Deganello, J. Phys. Chem. B 109 (2005) 2821–2827.
[27] D.R. Ou, T. Mori, F. Ye, M. Miyayama, S. Nakayama, J. Zou, G.J. Auchterlonie, J. Drennan, J. Electrochem. Soc. 156 (2009) B825–B830.